Lumenal gating mechanism revealed in calcium pump crystal structures with phosphate analogues

Chikashi Toyoshima, Hiromi Nomura* & Takeo Tsuda

[1]*Institute of Molecular and Cellular Biosciences, The University of Tokyo, Bunkyo-ku, Tokyo 113-0032, Japan*

* Present address: Department of Information Physiology, National Institute for Physiological Sciences, Okazaki 444-8787, Japan

P-type ion transporting ATPases are ATP-powered ion pumps that establish ion concentration gradients across biological membranes. Transfer of bound cations to the lumenal or extracellular side occurs while the ATPase is phosphorylated. Here we report at 2.3 Å resolution the structure of the calcium-ATPase of skeletal muscle sarcoplasmic reticulum, a representative P-type ATPase that is crystallized in the absence of Ca^{2+} but in the presence of magnesium fluoride, a stable phosphate analogue. This and other crystal structures determined previously provide atomic models for all four principal states in the reaction cycle. These structures show that the three cytoplasmic domains rearrange to move six out of ten transmembrane helices, thereby changing the affinity of the Ca^{2+}-binding sites and the gating of the ion pathway. Release of ADP triggers the opening of the lumenal gate and release of phosphate its closure, effected mainly through movement of the A-domain, the actuator of transmembrane gates.

Cation pumps that establish ion gradients across biological membranes belong to the P-type ATPase superfamily. This includes Na^+K^+-ATPase, gastric H^+K^+-ATPase and other important ion pumps (see refs 1 and 2 for reviews). According to the classical E1/E2 theory[3–5], active transport by P-type ATPases is achieved by alternating the affinity and accessibility of the transmembrane ion binding sites: they have high affinity for the activating ion in E1 and low affinity in E2; they face the cytoplasm in E1 and the lumen or extracellular medium in E2. Actual transfer of the activating ion takes place while the ATPase is phosphorylated at an aspartyl residue. That is, bound ions occluded in the transmembrane binding sites in E1P·ADP and E1P are released into the lumen (or outside of the cell) during the transition to E2P. At the same time, the ADP-sensitivity, that is, the ability of the phosphoenzyme to synthesize ATP from ADP, is lost. Hydrolysis of the aspartylphosphate completes the cycle.

In the P-type ATPase family, Ca^{2+}-ATPase of skeletal muscle sarcoplasmic reticulum (SERCA1a) is structurally and functionally the best studied member. It consists of a single polypeptide of 994 amino acid residues[6,7], and comprises three cytoplasmic domains designated as A (actuator), N (nucleotide) and P (phosphorylation) domains and 10 transmembrane helices[8]. We have previously determined its crystal structures in three states (reviewed in ref. 9). They are a Ca^{2+}-bound form (E1·2Ca^{2+}, Protein Data Bank (PDB) accession code 1SU4)[8], a Ca^{2+}-unbound form stabilized by a very potent inhibitor thapsigargin (TG) (E2(TG), PDB accession code 1IWO)[10], and a Ca^{2+}, Mg^{2+} and adenosine 5′-(β,γ-methylene)triphosphate (AMPPCP)-bound form (E1·AMPPCP, PDB accession code 1VFP)[11]. In the E1·AMPPCP structure, also solved by Sørensen *et al.*[12] (PDB accession code 1T5S), the γ-phosphate of AMPPCP, a non-hydrolysable analogue of ATP, is bound to Asp 351, the residue to be phosphorylated. Sørensen *et al.*[12] also determined an E1·AlF_4·ADP structure (PDB accession code 1T5T), which probably mimics an E1P·ADP state with AlF_4 as a stable phosphate analogue[13]. The structures of E1·AMPPCP and E1·AlF_x·ADP are virtually the same, with the bound Ca^{2+} occluded in the transmembrane binding sites[11,12].

Here we describe a crystal structure of the Ca^{2+}-ATPase with a bound phosphate analogue[14], MgF_4^{2-}, in the absence of Ca^{2+} at 2.3 Å resolution. This structure, abbreviated as E2·MgF_4^{2-}, contains Mg^{2+} next to the phosphate analogue and is stabilized with TG, as in the E2 crystals[10]. The structure appears to represent a state E2·P_i (refs 15, 16), just after the hydrolysis of the aspartylphosphate but before the release of phosphate from the ATPase. We compare this structure with our own model of E1·AlF_x·ADP at 2.7 Å resolution and that of E2(TG)[10] at 3.1 Å resolution (Fig. 1).

Thus, the structures described here are not exact analogues of E1P and E2P, but have very close domain organizations as revealed by limited proteolysis[15,17]. They show how the affinity of the transmembrane Ca^{2+} binding sites is altered, and how the lumenal gate is opened and closed by events that occur around the phosphorylation site some 50 Å away. A fairly complete description of the entire transport cycle is now possible. We show that the orientation of the A-domain plays the key role in regulating the transmembrane gates.

Structure determination

Crystals of E1·AlF_x·ADP complex were formed only with a *C*2 symmetry and showed very similar unit cell parameters to those of E1·AMPPCP crystals[11]. The structure was determined by generalized molecular replacement[18] from the model built for E1·AMPPCP and refined at 2.7 Å resolution.

Ca^{2+}-ATPase forms a very stable complex[14,19] with Mg^{2+} and F^- in the absence of Ca^{2+}. Crystals of two different symmetries formed but only in the presence of thapsigargin. The crystals of *C*2 symmetry diffracted to 2.9 Å resolution. An initial rough atomic model was built without much difficulty using generalized molecular replacement[18], starting from the three cytoplasmic domains of E1·2Ca^{2+} fitted into a low-resolution (8 Å) map[8] derived by electron microscopy for vanadate-induced tubular crystals[20]. This model was used for molecular replacement with the crystals of $P2_1$ symmetry, which contained four molecules in the asymmetric unit. The atomic model was refined at 2.3 Å resolution to an R_{free} of 24.8%. At this resolution it was clear that the bound phosphate analogue is MgF_4^{2-}, rather than MgF_3^- as in a Rho protein[21] (Supplementary Fig. 1). Because one Mg^{2+} is also bound between Asp 351 and Asp 703, the

©2004 Nature Publishing Group

stoichiometry of Mg^{2+} and F^- agrees well with biochemical measurements[22,23]. The differences among the four molecules were small. During the course of preliminary model building, ADP, introduced in the purification procedure[24,25], was observed in the structure. ADP was therefore included in the crystallization buffer for $P2_1$ crystals.

Overview of the structural changes

In all of the three structures compared here, the three cytoplasmic domains adopt overall compact forms. The arrangement in E2·MgF_4^{2-}, however, is distinctly different from that in E1·AlF_x·ADP (Fig. 1). The A-domain is ~110° rotated around an axis approximately perpendicular to the membrane (Fig. 2a, b) passing near

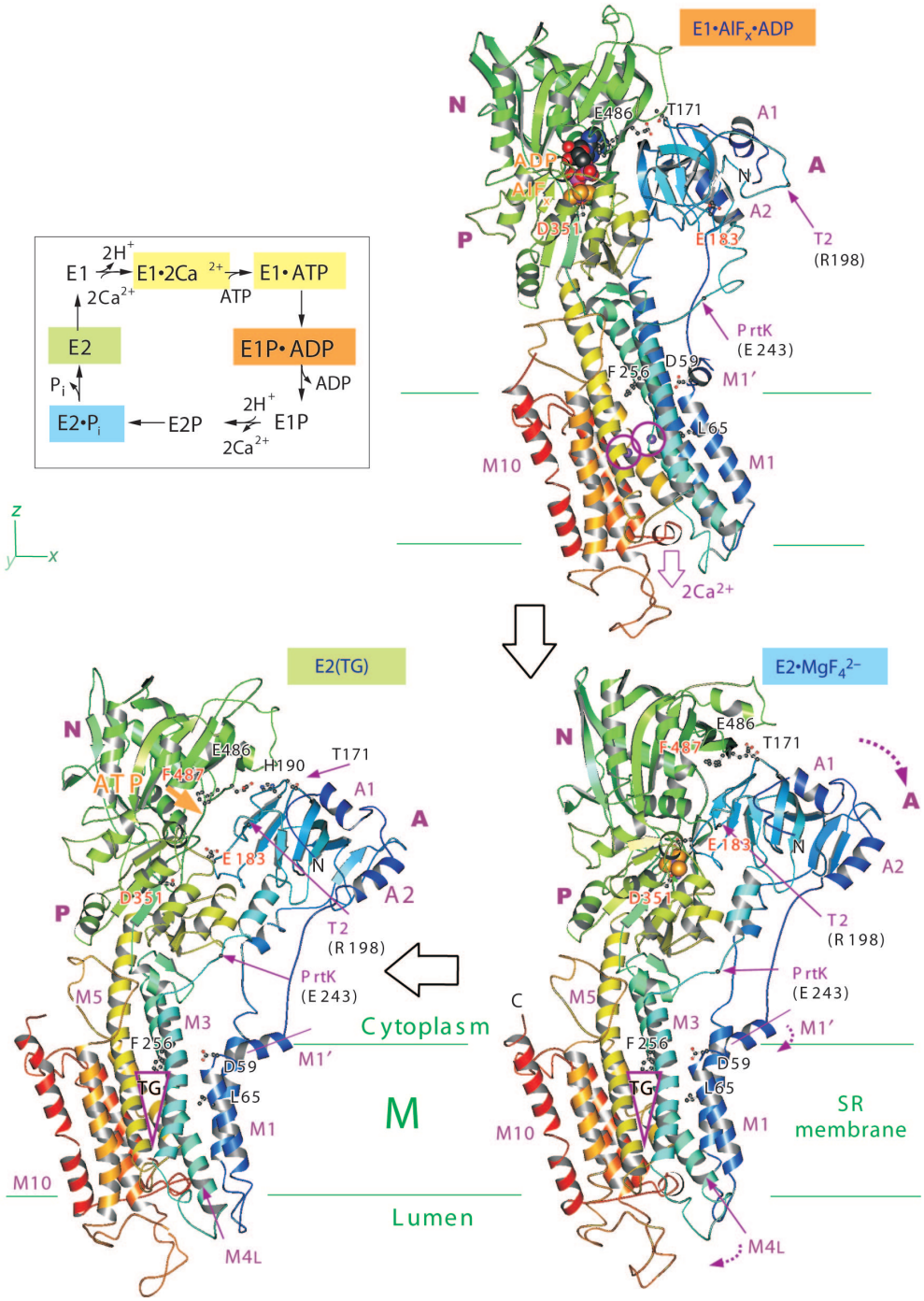

Figure 1 Front views (parallel to the membrane (*x*–*y*) plane) of Ca^{2+}-ATPase in three different states and a simplified reaction scheme (showing only the forward direction), in which different colours correspond to the respective structures presented here. The states whose names have yellow background refer to those previously described. In the ribbon models, colours change gradually from the amino terminus (blue) to the carboxy terminus (red). Purple spheres (circled) represent bound Ca^{2+}. Three cytoplasmic domains (A, N and P), the α-helices in the A-domain (A1 and A2) and those in the transmembrane domain (M1, M4L, M5 and M10) are indicated. M1′ is an amphipathic part lying on the bilayer surface. PrtK, a proteinase-K digestion site (around Glu 243 (ref. 45)); SR, sarcoplasmic reticulum; T2, a trypsin digestion site at Arg 198 (ref. 7); ATP, the binding pocket for the adenosine moiety of ATP; TG, thapsigargin. Several key residues—E183 (A), F487 (N, adenine binding), D351 (P, phosphorylation site), D59, L65 (M1) and F256 (M3, TG binding)—and those involved in interdomain hydrogen bonds (including T171, H190 and E486), are shown in ball-and-stick representation. Prepared with Molscript[46]. Secondary structure was assigned with DSSP (ref. 47).

©2004 Nature Publishing Group
NATURE | doi:10.1038/nature02981 | www.nature.com/nature

Val 705 in the P-domain, the residue forming a platform for tilting of the A-domain in the E1·2Ca^{2+} → E1·AMPPCP transition. Tight association of the A- and P-domains is achieved through bound MgF_4^{2-} and Mg^{2+} (see later) and stabilized by several hydrogen bonds (including those between Arg 198 and Asp 660 and between Asp 203 and Arg 678 (Fig. 2c, inset)). Compared with E1·AlF_x·ADP, the N-domain associates with the P-domain very weakly, moved away from the P-domain by ~60°. This is because the bridges between the N- and P-domains, facilitated by the ADP moiety of ATP[11], are lost and the A-domain wedges into the space. The interface between the N- and A-domains is also loose (Figs 1 and 2) and only two hydrogen bonds can be identified. The one between Thr 171 (A) and Glu 486 (N) is present also in E1·AlF_x·ADP, forming a mechanical couple (refer to Fig. 6 of ref. 11).

Reflecting these differences in the organization of cytoplasmic domains, the transmembrane helices M1–M6 are markedly rearranged between E1·AlF_x·ADP and E2·MgF_4^{2-} (Figs 3a, b and 4a). The M3 and M4 helices are moved one turn of an α-helix towards the lumen (Fig. 3a, b); the M5 helix is bent towards M1 (Fig. 1), tilting the P-domain ~30° with respect to the membrane plane. These rearrangements, resulting in the release of Ca^{2+} into the lumen of the sarcoplasmic reticulum, are similar to those described previously for the E1·2Ca^{2+} → E2(TG) transition[10].

This similarity arises because the arrangements of the cytoplasmic domains and transmembrane helices are similar in E2·MgF_4^{2-} and E2(TG)[10] (Fig. 1). For example, the path of the M5 helix and that of the cytoplasmic part of M4, which have principal roles in changing the affinity of the transmembrane Ca^{2+}-binding sites[10], are virtually the same (Fig. 2d). Thus, the structure around the Ca^{2+}-binding sites hardly changes. The lumenal half of the M4 helix (M4L), however, shows a ~20° difference in inclination (Figs 1, 3c and 4b), apparently closing the lumenal gate in E2(TG). This movement of M4L is related to that of the A-domain, which tilts ~30° with respect to the membrane plane (Figs 1 and 2d). This movement is caused by the release of Mg^{2+} and MgF_4^{2-}, which relaxes the P-domain and makes ineffective the secondary hinge in the β-sheet in the P-domain[11]; as a result, the N-domain also changes its inclination (~30°), forming a different interface with the A-domain (Fig. 1).

Structure around the phosphorylation site

The most characteristic feature in E2·MgF_4^{2-} is a tight association of the A- and P-domains. The structure of the P-domain itself is virtually unaltered from E1·AMPPCP to E2·MgF_4^{2-}. Given the high similarity in the P-domain structure between E1·2Ca^{2+} and E2(TG)[10], this means that the P-domain of Ca^{2+}-ATPase assumes,

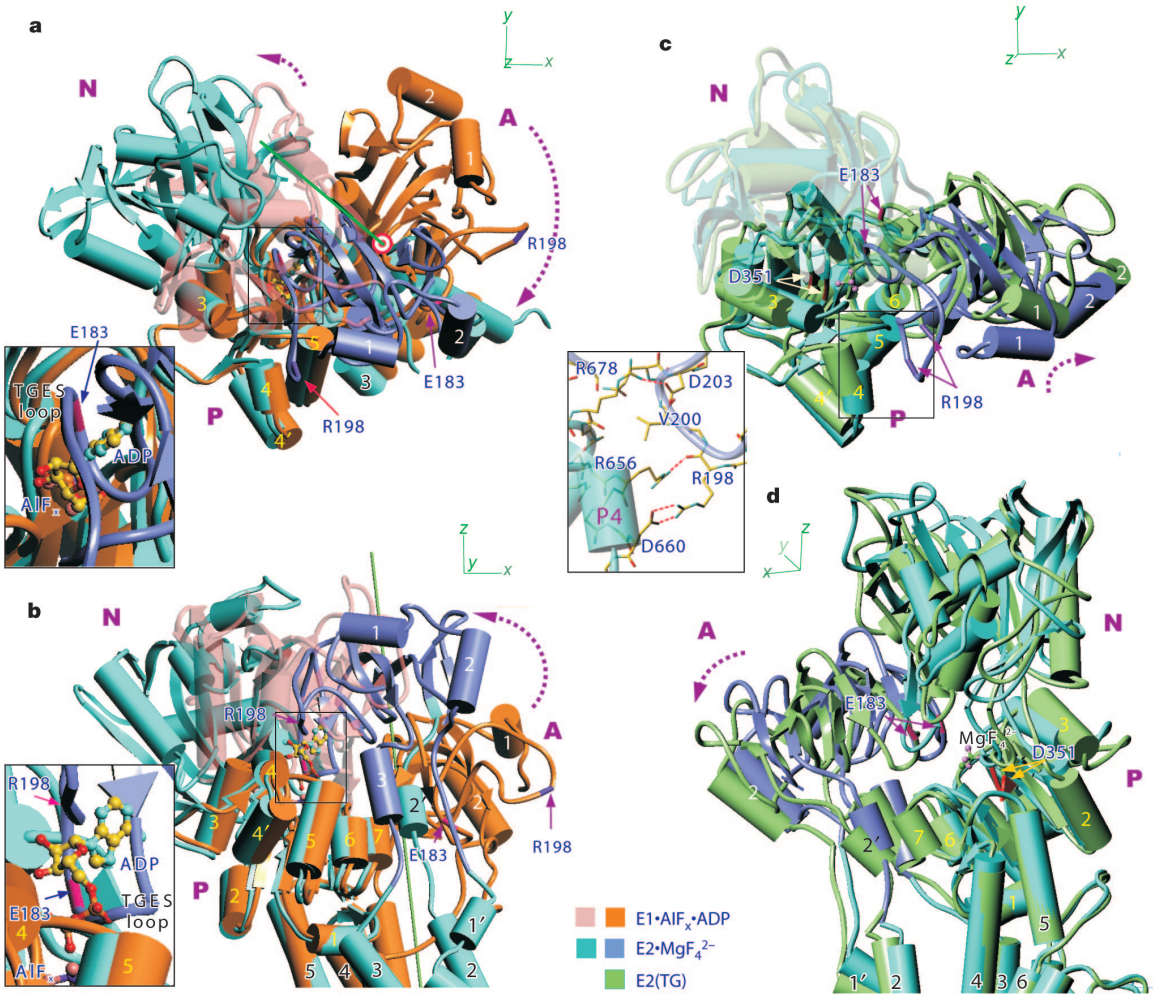

Figure 2 Movements of the cytoplasmic domains. The cytoplasmic domains of the E2·MgF_4^{2-} complex are superimposed with those of E1·AlF_x·ADP (**a**, **b**) and E2(TG) (**c**, **d**), aligned with the top part of the M5 helix integrated in the P-domain. Viewing directions are specified with *x*, *y*, *z* axes. Insets in **a** and **b** show the area around the phosphorylation site (Asp 351, coloured red in **c** and **d**); the one in **c** shows the interface between the A- and P-domains around Arg 198. Ligands are shown in ball-and-stick representation. Different colours are used for the A-domain in E2·MgF_4^{2-} and the N-domain in E1·AlF_x·ADP (transparent in **a** and **b**), to make the A-domain/N-domain interaction clearer. Large dotted arrows show the directions of expected movements in E1P → E2P and E2P → E2.

©2004 Nature Publishing Group

as a first approximation, only two distinct structures depending on the phosphorylation state (or γ-phosphate binding). In E2·MgF_4^{2-}, the TGES signature sequence starting from Thr 181 (ref. 26) in the A-domain now participates in the coordination of MgF_4^{2-} and Mg^{2+} (Fig. 5), associating the A- and P-domains tightly. In E1·2Ca^{2+} to E1·AlF_x·ADP, this sequence is located on the outermost surface of the ATPase, but brought into the phosphorylation site by the A-domain rotation (Figs 1 and 2a, b).

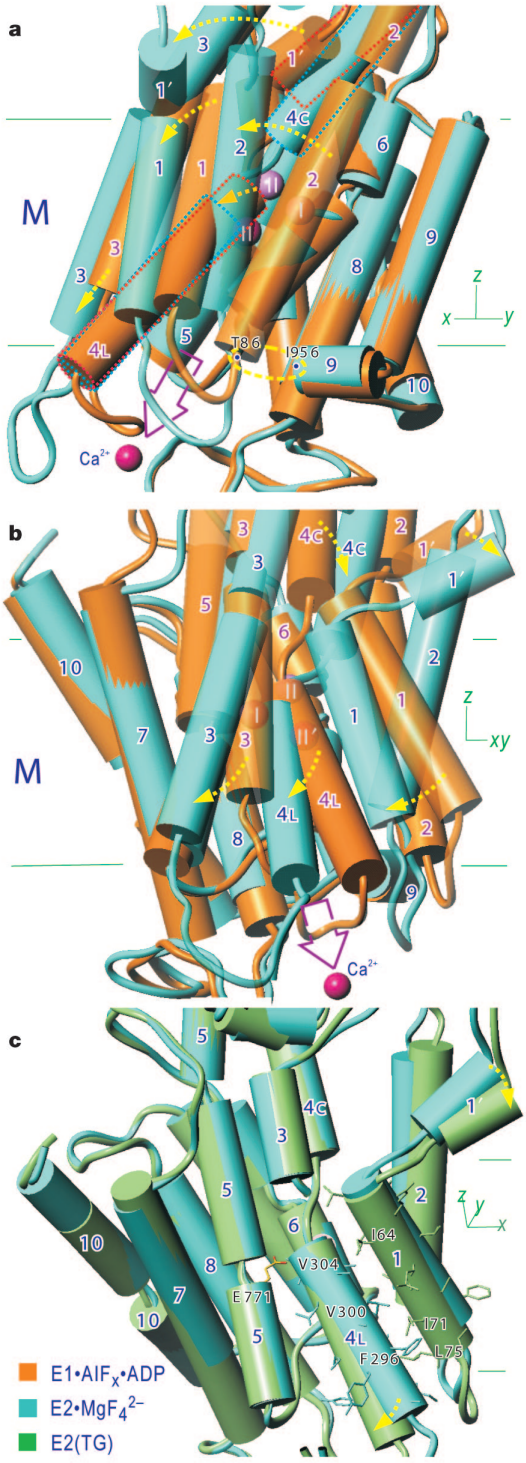

Figure 3 Movements in the transmembrane domain. The transmembrane domain of E2·MgF_4^{2-} is superimposed with E1·AlF_x·ADP (**a**, **b**) and E2(TG) (**c**), and viewed along the membrane plane. Transmembrane helices are numbered. Yellow arrows show the directions of movements in E1·AlF_x·ADP → E2·MgF_4^{2-} (**a**, **b**) and E2·MgF_4^{2-} → E2(TG) (**c**). Positions of Ca^{2+} in E1·AlF_x·ADP are shown together with that expected (II′) for site II Ca^{2+} after transition to E2·MgF_4^{2-} (**a**, **b**). Positions of the two halves of M4 (M4C and M4L) are outlined with dotted lines (**a**). Large open arrows indicate the release of Ca^{2+} into the lumen.

Of these four well-conserved and mutation-sensitive[27] residues in the TGES motif, Gly 182 and Glu 183 have clear functional roles. The carbonyl group of Gly 182 is located above the Mg^{2+} bound to Asp 703 and contributes to its binding through a water molecule (Fig. 5). This water molecule is also present in E1·AMPPCP[11,12] and E1·AlF_x·ADP[12] but not fixed from above. The contribution of Gly 182 explains the higher affinity of the divalent metal at this site in E2P than in E1P[28]. Glu 183 has one of its carboxyl oxygens at a hydrogen bond distance from a fluorine in MgF_4^{2-} (Fig. 5). Considering the high electronegativity of fluorine, this configuration will be unstable unless that carboxyl oxygen is protonated. This in turn suggests that the carboxyl of Glu 183 is forced into this position by surrounding structure.

The importance of Glu 183 may be understood by considering the phosphorylated structure. As mentioned earlier, the structure of E2·MgF_4^{2-} probably represents that of E2·P_i, immediately after the hydrolysis of the aspartylphosphate[16]. An atomic model of an aspartylphosphate can be taken from that of CheY (PDB accession code 1QMP)[29], a bacterial response regulator, which uses identical residues for the stabilization of phosphoryl group and Mg^{2+} despite the different protein folding pattern[30]. In Fig. 5b, the model of aspartylphosphate is superimposed with the main chain to Asp 351. The oxygens of the phosphoryl group of the aspartylphosphate superimposed on the fluorines of MgF_4^{2-} without any change in the side-chain conformation of Asp 351. The aspartylphosphate does not have an oxygen atom corresponding to the distal fluorine, which is presumably hydrogen-bonded to Glu 183 in Ca^{2+}-ATPase. It is therefore likely that a water molecule normally occupies this position, at a distance of 2.8 Å from the carboxyl oxygen of Asp 351 (Fig. 5b), fixed by Glu 183 and the carbonyl of Thr 181, and makes an in-line attack on the aspartylphosphate to initiate hydrolysis (Fig. 5b). A mutagenesis study showed that Glu 183 is critical for E2P hydrolysis and phosphorylation from P_i (ref. 31).

Then, accurate positioning of Glu 183 will be paramount. Its carboxyl group is fixed by hydrogen bonds with Thr 353, a crucial residue[32,33], and indirectly through a water molecule with Asp 601 in the hinge region (Fig. 5). Stabilization of the TGES loop itself through the Thr 181 hydroxyl group may also be important, as mutagenesis studies demonstrated[27]. Hydrogen bonds between Ser 184 and Asn 359 in the hinge region, and between Ser 186 and Glu 439 in the N-domain, will also contribute. Furthermore, Gly 182 is bound to Mg^{2+} through a water molecule. This may be critical for decreasing the chance of a back reaction because the release of phosphate will release Mg^{2+}, which in turn will destabilize the TGES loop.

Roles of ADP-release

As described previously[11], there is a large space, presumably filled with bulk water, around the γ-phosphate of AMPPCP bound to Asp 351. This space is occupied by the A-domain in E2·MgF_4^{2-}, in particular, with the hairpin containing the TGES signature sequence (Fig. 2a, b, inset). In fact, this hairpin occupies the space taken by ADP in E1·AlF_x·ADP. The TGES loop protrudes deeply into the P/N interface and probably even more so in genuine E2P with the smaller aspartylphosphate (Fig. 5b).

The binding of ADP is allowed in E2·MgF_4^{2-} (Supplementary Fig. 2; ref. 23) because the binding pocket for the adenine ring (around Phe 487) in the N-domain is still available. Mg^{2+} appears to bridge α- and β-phosphates without ligating protein, as in E1·AlF_x·ADP. However, ADP is prevented from interacting with the phosphorylation site by the TGES loop (Supplementary Fig. 2) and synthesis of ATP in the reverse reaction is prohibited. This

©2004 Nature Publishing Group
NATURE | doi:10.1038/nature02981 | www.nature.com/nature

feature explains the ADP-insensitivity of E2P. One of the differences of E2·MgF_4^{2-} from E2P is that the superfluorescence of TNP-AMP, characteristic of the nucleotide bound to E2P, is not observed with E2·MgF_4^{2-} (ref. 16). Deeper penetration of the TGES loop in genuine E2P could confine the space for nucleotide, and steric factors could play a part in the modulations of the reactions of E2P and E2·Pi by ATP[34,35].

Then the question arises: in the transition from E1P·ADP to E2P, does the TGES loop directly remove the ADP from the binding site? This seems unlikely, because the large rotation of the A-domain is only possible after the relaxation of the N-domain–P-domain association. In E1·AMPPCP and E1·AlF_x·ADP, β-phosphate seems to be critical for keeping the N-domain in the highly inclined position[11]. Thus, the trigger for the transition into E2P is likely to be the release of ADP.

Release of Ca^{2+} into the lumen

In the E1P ⟶ E2P transition, the transmembrane helices undergo marked rearrangement. This rearrangement is essentially the same as in E1·2Ca^{2+} ⟶ E2(TG)[10] in that the movements of the M3 and M4 helices have large downward components perpendicular to the membrane plane (Fig. 3a, b) apparently pushing out the Ca^{2+}, and in that the M5 helix bends substantially towards M1 (Fig. 1). These movements are mechanically linked, as described previously[10], and decrease the number of oxygen atoms that can participate in the coordination of Ca^{2+}, thereby lowering the affinity for Ca^{2+}. The geometry of coordinating residues changes more markedly at site II (ref. 10), in which main-chain carbonyls of Val 304, Ala 305, Ile 307 (M4) and side-chain oxygens of Asn 796, Asp 800 (M6) and Glu 309 (M4) contribute in E1·2Ca^{2+} (ref. 8).

There is a critical difference between E2·MgF_4^{2-} and E2(TG), however, relating to the release of Ca^{2+}, because the E1·2Ca^{2+} ⟶ E2 transition (backward reaction) releases Ca^{2+} into the cytoplasm whereas the transition into E2P (forward reaction) releases Ca^{2+} into the lumen by opening the lumenal gate. The structure around the transmembrane Ca^{2+}-binding sites is depicted in Fig. 4, in which the positions of the Ca^{2+} in E1·AlF_x·ADP (I and II, violet spheres) are shown together with the expected position of site II Ca^{2+} immediately after the transition into E2P (II′, red sphere). In E1·AlF_x·ADP, the lumenal half of the M4 helix (M4L, orange tube) comes closest to M6 near the Ca^{2+} at binding site II. Although displaced, site II Ca^{2+} is still almost on M4L, coordinated by the main-chain carbonyl of Val 304. In E2·MgF_4^{2-} (blue structure), M4L becomes parallel to M6, and forms a smooth interface devoid of bulky residues (Fig. 4b). If the site II Ca^{2+} moves together with Glu 309, which is suggested from the similar conformation in either state, it will come into the space between M4 and M6. This is because M4L changes its orientation relative to the loop containing Glu 309 (Figs 3b and 4a); the cytoplasmic part of M4 (M4C) is pushed towards M1 by M5 (ref. 10) whereas M4L is pushed by M1 in a different direction (Figs 3b and 4a).

Here the Ca^{2+} (II′) meets Val 304, a well-conserved residue, Ala 301 or Leu 792 and must pass through the space surrounded by the M4 to M6 helices to reach the lumen (Fig. 4b; Supplementary Fig. 3). The side-chain nitrogen of Asn 796 comes close to the Ca^{2+}. This disposition, stabilized by hydrogen bonds with Glu 771, may help release Ca^{2+} into the lumen and block the entry of cations (other than H^+ to be countertransported) from the lumenal side. It is interesting that this residue is aspartic acid in Na^+K^+- and H^+K^+-ATPases, which countertransport K^+ rather than H^+.

We must remember, however, that the lumenal gate is probably not fully open in E2·MgF_4^{2-}: a high concentration of Ca^{2+} (>mM) and a long time (>min) are required to reactivate the pump[14]. Also, the fluorescence from the tryptophans in the transmembrane region of E2·MgF_4^{2-} is largely diminished to a level similar to E2 (ref. 16). In genuine E2P, the passage is presumably wider. One way for predicting the structure in genuine E2P will be an extrapolation of the movement in E2(TG) ⟶ E2·MgF_4^{2-}. In E2·MgF_4^{2-} ⟶ E2(TG), as described earlier, the release of the A-domain causes a movement of M4L (Figs 1, 3c and 4b) and decreases the space surrounded by M4–M6 helices (Fig. 4b). Thus, the exit channel is closed. In genuine E2P, the A-domain will be more tilted than in E2·MgF_4^{2-} towards the phosphorylation site and so will M1–M2, locating the lumenal end of M4L further away from M5 and M6. In such a position, the space surrounded by M4–M6 will be larger and will allow Ca^{2+} to pass through.

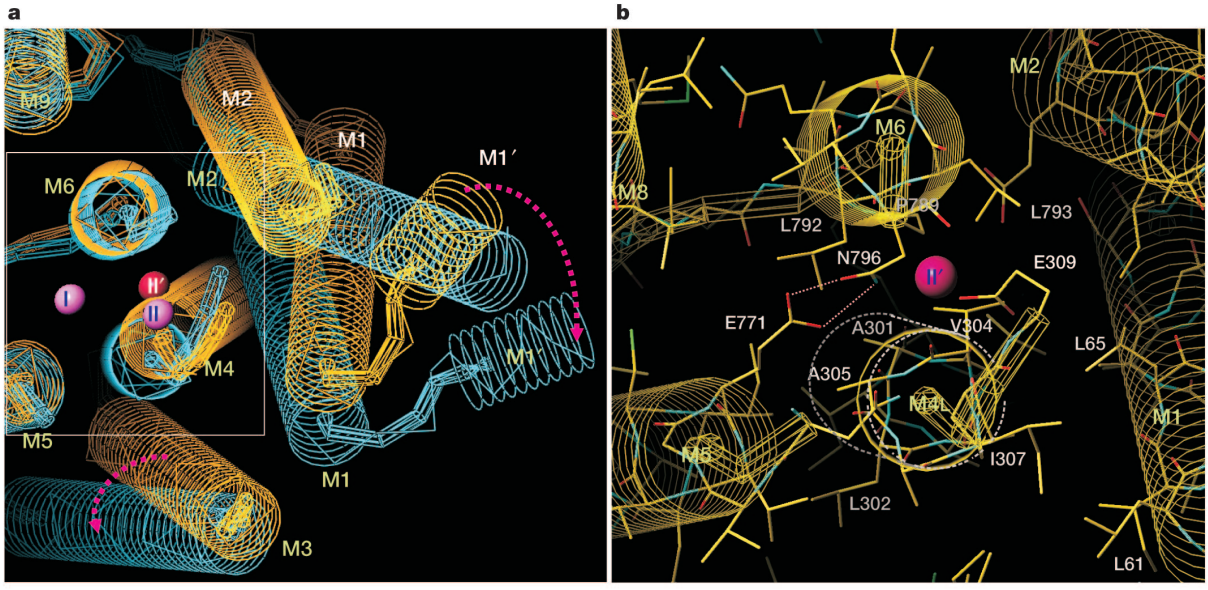

Figure 4 Movements in the transmembrane domain viewed approximately normal to the membrane plane from the cytoplasmic side. Superimposition of the transmembrane domains of E2·MgF_4^{2-} and E1·AlF_x·ADP (**a**) and details in E2·MgF_4^{2-} (**b**) of the boxed area in **a**. Spheres in violet show the Ca^{2+} in E1·AlF_x·ADP and those in red the expected position of Ca^{2+} after transition to E2·MgF_4^{2-}. Arrows in **a** show the movements of transmembrane helices in E1·AlF_x·ADP ⟶ E2·MgF_4^{2-}. The cylinder outlined by a dashed line in **b** outlines the M4L in E2(TG).

©2004 Nature Publishing Group

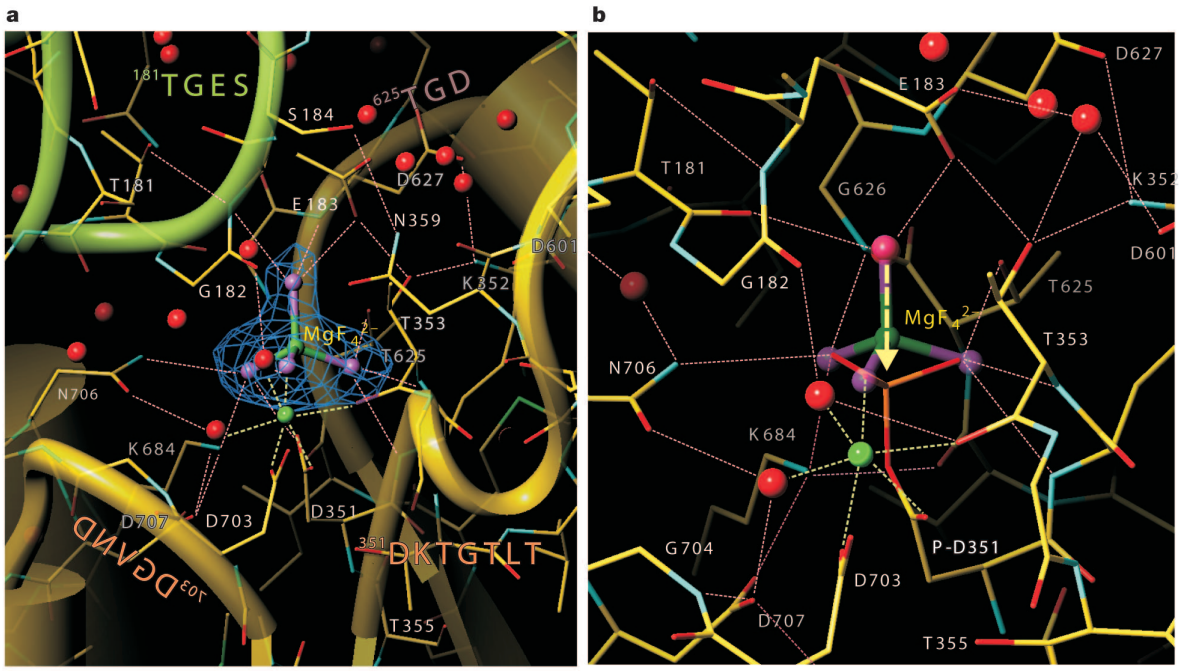

Figure 5 Details of the phosphorylation site in E2·MgF_4^{2-}. In the enlarged view (**b**), the atomic model of aspartylphosphate taken unchanged from a related protein CheY (PDB accession code 1QMP)[29] is incorporated. The blue net in **a** shows an omit annealed Fo–Fc map (at 5σ; temperature factor also refined) at 2.3 Å resolution. Small spheres represent water molecules (red) and Mg^{2+} (green). MgF_4^{2-} is shown in ball-and-stick representation. Large yellow arrow indicates the expected water attack to the aspartylphosphate (P-D351). Conserved sequence motifs are shown in **a**. Broken lines in pink indicate likely hydrogen bonds, and those in light green coordinations of Mg^{2+}.

Links between the A-domain and transmembrane helices

Large movements of the transmembrane helices are linked to even larger rearrangements of the cytoplasmic domains. The rotation of the A-domain is likely to be triggered by the strain imposed on the M3–A-domain link, which is stretched by more than 3 Å (for Ala 240-Thr 247) in E1·AlF_x·ADP. The rotation appears to be stabilized by electrostatic interactions involving the Arg 198-Asp 202 loop (A-domain) and several charged residues in the P- and N-domains (Fig. 2c, inset). Positioning of this A-domain loop must be critical because mutations to Val 200 in the middle of this loop, which appears to orient long side chains of arginine and glutamic acid correctly and maintain them at optimal distances (Fig. 2c, inset), almost completely abolish ATPase activity[36].

The next question to ask is how the A-domain rotation is transmitted to the transmembrane helices. One interesting feature here is that the V-shaped structure formed by M1 (including M1′) and M2 helices move as a rigid body. M1 has extensive van der Waals contacts with M2 and M4L (Fig. 3). Although M4L and M1 do not move as a rigid body, they keep the same van der Waals contacts from E1·AMPPCP to E2(TG). Because M2 is a long continuous helix in E1·$2Ca^{2+}$ and pulled towards the A-domain in E1·$2Ca^{2+}$ → E1·AMPPCP, M2 is expected to have a firm interaction with the A-domain suitable for transmitting the movement of the A-domain to the transmembrane part. Then M1 will be able to move M4L with van der Waals contacts. In fact, the movement of the M1–M2 helices between E1·AlF_x·ADP and E2·MgF_4^{2-} can be regarded as a tilt of the V-shaped structure with the pivoting point around Thr 86 (at the lumenal end of M2) and Ile 956 (on a short helix connecting M9 and M10 helices; Fig. 3a).

Rotation of the A-domain will tilt the M1–M2 helices, because M1 is already in contact with M4L, which cannot move much towards M5 or M6 due to steric collisions (Fig. 4a). Hence, the directions of the movement of M1 and M4 are similar (Figs 3a, b and 4a) but modified by their respective steric constraints. Because this is a tilting movement bringing the V-shaped structure more upright (Fig. 3a), the movement has a component normal to the membrane (3.5 Å at Asp 59 on M1; 3.3 Å at Pro 308 on M4; Fig. 3a, b). In the E2·MgF_4^{2-} → E2(TG) transition, it is easier to see the correlation between the movements of the V-shaped structure and M4L (Fig. 3c).

Limited proteolysis and mutagenesis studies also provide some

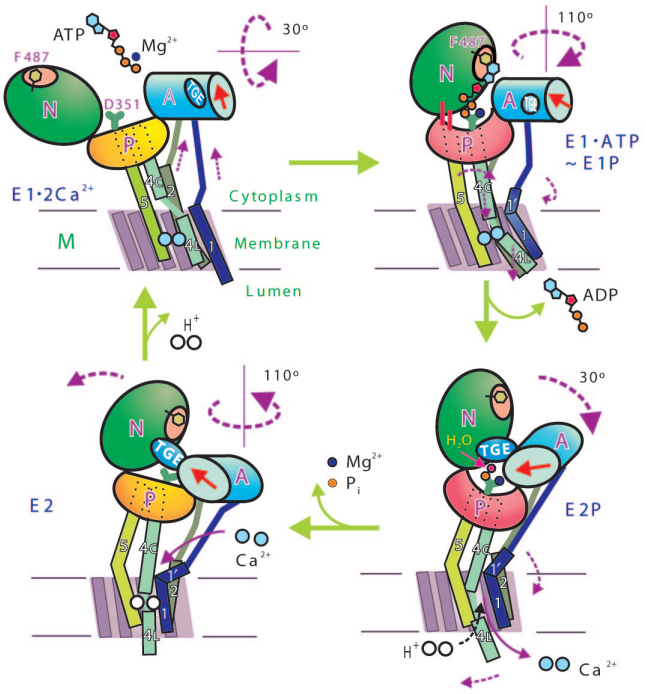

Figure 6 A cartoon depicting the structural changes of the Ca^{2+}-ATPase during the reaction cycle, based on the crystal structures in five different states.

©2004 Nature Publishing Group
NATURE | doi:10.1038/nature02981 | www.nature.com/nature

clues. A nick at Lys 120 located at the C-terminal end of M2 substantially slows the E2P → E2 transition but not E1P → E2P (ref. 37). Likewise, mutations of Tyr 122 block the E2P → E2 transition but not E1P → E2P (ref. 38). Thus, the route through M2 appears critical in E2P → E2 transition and less so in E1P → E2P.

In E1P → E2P, the connection to the A-domain through M3 seems to be more important, because a cleavage at Thr 242 on the loop (Fig. 1) strongly slows this transition[39]. In addition, the top part of M3 seems to be strained in E1·AlF_x·ADP, bent towards M2[11], but not in E2·MgF_4^{2-}. This strain will be removed if the P-domain inclines and bends the M5 helix towards M1. These are certainly the movements required for releasing bound Ca^{2+} to the lumen. Mutagenesis studies suggest that links through M2 as well as the P-domain are also important. Arg 324 and Arg 334 on M4 are critical in the E1P → E2P transition[38]. Arg 324 forms hydrogen bonds with Asn 101 and Gln 108 on M2 and Arg 334 with the P-domain in E1·AlF_x·ADP. Thus, for concerted movements of different parts, all these mechanical links seem to come into play.

Discussion

We now have five crystal structures that represent different states of the reaction cycle of Ca^{2+}-ATPase. They allow us to propose a synopsis of ion pumping (Fig. 6; Supplementary Movie).

(1) Ca^{2+} binding to E2, which is the ground state, straightens the M5 helix and breaks the closed configuration of the three cytoplasmic domains, exposing the catalytic site. Two Ca^{2+} are bound in the high affinity sites formed by transmembrane helices M4, M5, M6 and M8 (ref. 8). The cytoplasmic gate is open and bound Ca^{2+} exchange with those in the cytoplasm[40]. The M1 helix is deeply embedded in the lipid bilayer, stabilized indirectly by the bound Ca^{2+}.

(2) ATP binds and crosslinks the P- and N-domains, so that the γ-phosphate of ATP and a Mg^{2+} bind to the P-domain to bend it[11]. The N-domain is fixed in a highly inclined position and makes contact with the A-domain in a strained position. The M1 helix is pulled up and bent so that the top of the transmembrane part closes the cytoplasmic gate of the Ca^{2+} binding sites.

(3) Phosphoryl transfer to Asp 351 allows the dissociation of ADP, which triggers the opening of the N- and P-domain interface; the A-domain rotates so that the TGES loop wedges into the gap and interacts with the phosphorylation site. This causes a marked rearrangement of the transmembrane helices M1–M6; large downward movements of M4, sharp bending of M5 and rotation of M6 destroy the Ca^{2+}-binding sites[10]. The lower sections of M1 and M2 push against M4L, opening the lumenal gate and releasing the bound Ca^{2+} into the lumen.

(4) The TGES loop of the A-domain fixes a particular water molecule and catalyses its attack on the aspartylphosphate. The release of the phosphate and Mg^{2+} unbends the P-domain. This in turn releases M1 and M2 so that M4L closes the lumenal gate. The top amphipathic part of M1 (M1′) forms a part of a cytoplasmic access funnel leading to Glu 309 (ref. 10), the gating residue of the Ca^{2+} binding sites[41].

In short, the P- and N-domains change interfaces and thereby control the position of the A-domain, the actuator of transmembrane gates. ATP, phosphate, Mg^{2+} and Ca^{2+} are the modifiers of the interfaces. Energy barriers between the principal intermediate states seem to be comparable to the thermal energy, and we have seen devices integrated into Ca^{2+}-ATPase to decrease the chance of back reactions. Presumably the use of large-scale domain rearrangements, rather than small changes in the residues coordinating Ca^{2+}, is the means that nature has found to convert inherently stochastic thermal motions into concerted sequential movements with the help of ATP and the other modifiers. □

Methods

Crystallization

A MgF_4^{2-} complex of Ca^{2+}-ATPase was made by suspending sarcoplasmic reticulum vesicles in a buffer containing 1 mM KF, 10 mM $MgCl_2$, 1 mM EGTA, 20% DMSO, 20% glycerol and 50 mM MOPS, pH 7.1. Ca^{2+}-ATPase was solubilized with 2% octaethyleneglycol mono-*n*-dodecylether ($C_{12}E_8$) and purified by affinity chromatography as described[19,24,25], but in the absence of Ca^{2+}. For elution from the column, 4 mM ADP was used. Affinity purified enzyme (20 μM) in $C_{12}E_8$ was mixed with thapsigargin (30 μM), then dialysed against a buffer consisting of 2.75 M glycerol, 10–12% PEG 400, 5 mM $MgCl_2$, 3 mM KF, 0.06 mM ADP, 2.5 mM NaN_3, 2 μg ml^{-1} butylhydroxytoluene, 0.2 mM dithiothreitol, 1 mM EGTA, 20 mM MES, pH 6.1, for about one month. Crystals were grown to 300 × 300 × 50 μm and flash-frozen in cold nitrogen gas.

Crystals of E1·AlF_x·ADP were made by dialysing affinity purified enzyme against a buffer containing 2.75 M glycerol, 10–12% PEG 400, 2 mM $AlCl_3$, 6 mM NaF, 0.3 mM ADP, 1 mM $MgCl_2$, 0.2 M ammonium acetate, 3 mM $CaCl_2$, 2.5 mM NaN_3, 0.2 mM dithiothreitol, 2 μg ml^{-1} butylhydroxytoluene, 20 mM MES, pH 6.1. Crystals were grown to 200 × 100 × 50 μm.

Data collection

Diffraction data were collected at BL41XU of SPring-8 using MAR-165 CCD detector and Rigaku R-Axis V imaging plate detector. A part of the initial data set for E2·MgF_4^{2-} was obtained at BL44XU using DIP2040 imaging plate detector. Diffraction intensities from the three best crystals were merged for E2·MgF_4^{2-} (R_{merge} = 5.9%, I/σ = 25.1, redundancy = 5.1; 43.2%, 3.3, 2.0, respectively, for the highest resolution bin, 2.4–2.3 Å) and the two best crystals for E1·AlF_x·ADP using Denzo and Scalepack[42]. Unit cell parameters were: a = 102.2, b = 275.4, c = 109.9 Å and β = 90.01° for E2·MgF_4^{2-} crystals of $P2_1$ symmetry; a = 176.2, b = 70.0, c = 142.2 Å and β = 107.0° for E2·MgF_4^{2-} crystals of $C2$ symmetry; a = 163.1, b = 75.0, c = 151.5 Å and β = 109.3° for E1·AlF_x·ADP crystals.

Modelling

An initial model of E2·MgF_4^{2-} was built with the $C2$ crystals starting from the three cytoplasmic domains fitted into an 8 Å resolution map[8] derived by electron microscopy of vanadate induced tubular crystals[20]. PC-refinement[18] converged immediately and the calculated map showed that the P-domain was significantly different from that in E1Ca^{2+}. Then, the rest of the model was built gradually by many cycles of map calculation, solvent flattening[43] and manual model building. (See Supplementary Methods for more details.)

The final model was made with the $P2_1$ crystals, which contain four molecules in the asymmetric unit. PC-refinement after dividing the model of a monomer into 10 segments showed that the two molecules in the asymmetric unit form a pair. The largest differences between the pairs were observed with the uppermost loop (around Arg 505, T1 trypsin site) and the lumenal loop connecting M7 and M8 helices. The model includes four protomers, each of which contains Ca^{2+}-ATPase, TG, MgF_4^{2-}, $2Mg^{2+}$ and ADP, and altogether 594 water molecules. It was refined against the diffraction data consisting of 249,278 reflections (93.3% completeness) to R_{free} of 0.248 and R_{cryst} of 0.228 at 2.3 Å resolution; root mean square deviation (r. m. s. d.) of the bond length and angle were 0.007 Å and 1.2°, respectively.

The model of E1·AlF_x·ADP was built similarly to that of E1·AMPPCP (ref. 11). Because the two structures were virtually the same, the model built for E1·AMPPCP was used as the starting model in the refinement. The model included Ca^{2+}-ATPase, ADP, AlF_x, 2 Mg^{2+} and six water molecules. It was refined against the diffraction data consisting of 38,433 reflections. The modelling showed that both AlF_3 and AlF_4^- were possible with the map, as is the case with phosphoserine phosphatase[44], although the lack of electron density connecting the Mg^{2+} bound to ADP and the fourth fluorine in AlF_4^- (ref. 12) favours AlF_3. The model including AlF_3 gave slightly better R_{free} (0.290; R_{cryst} = 0.259) than AlF_4^- (R_{free} = 0.297; R_{cryst} = 0.258) at 2.7 Å resolution; r. m. s. d. of the bond length and angle were 0.009 Å and 1.4°, respectively.

Received 31 July; accepted 1 September 2004; doi:10.1038/nature02981.
Published online 26 September 2004.

1. Møller, J. V., Juul, B. & le Maire, M. Structural organization, ion transport, and energy transduction of P-type ATPases. *Biochim. Biophys. Acta* **1286,** 1–51 (1996).
2. Kühlbrandt, W. Biology, structure and mechanism of P-type ATPases. *Nature Rev. Mol. Cell Biol.* **5,** 282–295 (2004).
3. Albers, R. W. Biochemical aspects of active transport. *Annu. Rev. Biochem.* **36,** 727–756 (1967).
4. Post, R. L., Hegyvary, C. & Kume, S. Activation by adenosine triphosphate in the phosphorylation kinetics of sodium and potassium ion transport adenosine triphosphatase. *J. Biol. Chem.* **247,** 6530–6540 (1972).
5. de Meis, L. & Vianna, A. L. Energy interconversion by the Ca^{2+}-dependent ATPase of the sarcoplasmic reticulum. *Annu. Rev. Biochem.* **48,** 275–292 (1979).
6. Brandl, C. J., deLeon, S., Martin, D. R. & MacLennan, D. H. Adult forms of the Ca^{2+} ATPase of sarcoplasmic reticulum. Expression in developing skeletal muscle. *J. Biol. Chem.* **262,** 3768–3774 (1987).
7. MacLennan, D. H., Brandl, C. J., Korczak, B. & Green, N. M. Amino-acid sequence of a Ca^{2+} + Mg^{2+}-dependent ATPase from rabbit muscle sarcoplasmic reticulum, deduced from its complementary DNA sequence. *Nature* **316,** 696–700 (1985).
8. Toyoshima, C., Nakasako, M., Nomura, H. & Ogawa, H. Crystal structure of the calcium pump of sarcoplasmic reticulum at 2.6 Å resolution. *Nature* **405,** 647–655 (2000).
9. Toyoshima, C. & Inesi, G. Structural basis of ion pumping by Ca^{2+}-ATPase of the sarcoplasmic reticulum. *Annu. Rev. Biochem.* **73,** 269–292 (2004).
10. Toyoshima, C. & Nomura, H. Structural changes in the calcium pump accompanying the dissociation of calcium. *Nature* **418,** 605–611 (2002).

©2004 Nature Publishing Group

11. Toyoshima, C. & Mizutani, T. Crystal structure of the calcium pump with a bound ATP analogue. *Nature* **430,** 529–535 (2004).
12. Sørensen, T. L., Møller, J. V. & Nissen, P. Phosphoryl transfer and calcium ion occlusion in the calcium pump. *Science* **304,** 1672–1675 (2004).
13. Troullier, A., Girardet, J. L. & Dupont, Y. Fluoroaluminate complexes are bifunctional analogues of phosphate in sarcoplasmic reticulum Ca^{2+}-ATPase. *J. Biol. Chem.* **267,** 22821–22829 (1992).
14. Murphy, A. J. & Coll, R. J. Fluoride is a slow, tight-binding inhibitor of the calcium ATPase of sarcoplasmic reticulum. *J. Biol. Chem.* **267,** 5229–5235 (1992).
15. Danko, S. *et al.* ADP-insensitive phosphoenzyme intermediate of sarcoplasmic reticulum Ca^{2+}-ATPase has a compact conformation resistant to proteinase K, V8 protease and trypsin. *FEBS Lett.* **489,** 277–282 (2001).
16. Danko, S., Yamasaki, K., Daiho, T. & Suzuki, H. Distinct natures of beryllium fluoride-bound, aluminum fluoride-bound, and magnesium fluoride-bound stable analogues of an ADP-insensitive phosphoenzyme intermediate of sarcoplasmic reticulum Ca^{2+}-ATPase: changes in catalytic and transport sites during phosphoenzyme hydrolysis. *J. Biol. Chem.* **279,** 14991–14998 (2004).
17. Danko, S., Yamasaki, K., Daiho, T., Suzuki, H. & Toyoshima, C. Organization of cytoplasmic domains of sarcoplasmic reticulum Ca^{2+}-ATPase in E_1P and E_1ATP states: a limited proteolysis study. *FEBS Lett.* **505,** 129–135 (2001).
18. Brünger, A. T. Extension of molecular replacement: a new search strategy based on Patterson correlation refinement. *Acta Crystallogr. A* **46,** 46–57 (1990).
19. Yamasaki, K., Daiho, T. & Suzuki, H. Remarkable stability of solubilized and delipidated sarcoplasmic reticulum Ca^{2+}-ATPase with tightly bound fluoride and magnesium against detergent-induced denaturation. *J. Biol. Chem.* **277,** 13615–13619 (2002).
20. Zhang, P., Toyoshima, C., Yonekura, K., Green, N. M. & Stokes, D. L. Structure of the calcium pump from sarcoplasmic reticulum at 8-Å resolution. *Nature* **392,** 835–839 (1998).
21. Graham, D. L. *et al.* MgF_3^- as a transition state analog of phosphoryl transfer. *Chem. Biol.* **9,** 375–381 (2002).
22. Coll, R. J. & Murphy, A. J. Fluoride-inhibited calcium ATPase of sarcoplasmic reticulum. Magnesium and fluoride stoichiometry. *J. Biol. Chem.* **267,** 21584–21587 (1992).
23. Daiho, T., Kubota, T. & Kanazawa, T. Stoichiometry of tight binding of magnesium and fluoride to phosphorylation and high-affinity binding of ATP, vanadate, and calcium in the sarcoplasmic reticulum Ca^{2+}-ATPase. *Biochemistry* **32,** 10021–10026 (1993).
24. Coll, R. J. & Murphy, A. J. Purification of the CaATPase of sarcoplasmic reticulum by affinity chromatography. *J. Biol. Chem.* **259,** 14249–14254 (1984).
25. Stokes, D. L. & Green, N. M. Three-dimensional crystals of CaATPase from sarcoplasmic reticulum. Symmetry and molecular packing. *Biophys. J.* **57,** 1–14 (1990).
26. Palmgren, M. G. & Axelsen, K. B. Evolution of P-type ATPases. *Biochim. Biophys. Acta* **1365,** 37–45 (1998).
27. Clarke, D. M., Loo, T. W. & MacLennan, D. H. Functional consequences of mutations of conserved amino acids in the β-strand domain of the Ca^{2+}-ATPase of sarcoplasmic reticulum. *J. Biol. Chem.* **265,** 14088–14092 (1990).
28. Ogurusu, T., Wakabayashi, S. & Shigekawa, M. Activation of sarcoplasmic reticulum Ca^{2+}-ATPase by Mn^{2+}: a Mn^{2+} binding study. *J. Biochem.* **109,** 472–476 (1991).
29. Lewis, R. J., Brannigan, J. A., Muchova, K., Barak, I. & Wilkinson, A. J. Phosphorylated aspartate in the structure of a response regulator protein. *J. Mol. Biol.* **294,** 9–15 (1999).
30. Ridder, I. S. & Dijkstra, B. W. Identification of the Mg^{2+}-binding site in the P-type ATPase and phosphatase members of the HAD (haloacid dehalogenase) superfamily by structural similarity to the response regulator protein CheY. *Biochem. J.* **339,** 223–226 (1999).
31. Clausen, J. D., Vilsen, B., McIntosh, D. B., Einholm, A. P. & Andersen, J. P. Glutamate-183 in the conserved TGES motif of domain A of sarcoplasmic reticulum Ca^{2+}-ATPase assists in catalysis of E2/E2P partial reactions. *Proc. Natl Acad. Sci. USA* **101,** 2776–2781 (2004).
32. Maruyama, K. *et al.* Functional consequences of alterations to amino acids located in the catalytic center (isoleucine 348 to threonine 357) and nucleotide-binding domain of the Ca^{2+}-ATPase of sarcoplasmic reticulum. *J. Biol. Chem.* **264,** 13038–13042 (1989).
33. Clausen, J. D., McIntosh, D. B., Woolley, D. G. & Andersen, J. P. Importance of Thr-353 of the conserved phosphorylation loop of the sarcoplasmic reticulum Ca^{2+}-ATPase in MgATP binding and catalytic activity. *J. Biol. Chem.* **276,** 35741–35750 (2001).
34. McIntosh, D. B. & Boyer, P. D. Adenosine 5′-triphosphate modulation of catalytic intermediates of calcium ion activated adenosinetriphosphatase of sarcoplasmic reticulum subsequent to enzyme phosphorylation. *Biochemistry* **22,** 2867–2875 (1983).
35. Champeil, P. *et al.* ATP regulation of sarcoplasmic reticulum Ca^{2+}-ATPase. Metal-free ATP and 8-bromo-ATP bind with high affinity to the catalytic site of phosphorylated ATPase and accelerate dephosphorylation. *J. Biol. Chem.* **263,** 12288–12294 (1988).
36. Kato, S. *et al.* Val 200 residue in Lys 189-Lys 205 outermost loop on the A domain of sarcoplasmic reticulum Ca^{2+}-ATPase is critical for rapid processing of phosphoenzyme intermediate after loss of ADP sensitivity. *J. Biol. Chem.* **278,** 9624–9629 (2003).
37. Lenoir, G. *et al.* Functional properties of sarcoplasmic reticulum Ca^{2+}-ATPase after proteolytic cleavage at Leu 119-Lys 120, close to the A-domain. *J. Biol. Chem.* **279,** 9156–9166 (2004).
38. Yamasaki, K., Daiho, T., Danko, S. & Suzuki, H. Multiple and distinct effects of mutations of Tyr 122, Glu 123, Arg 324, and Arg 334 involved in interactions between the top part of second and fourth transmembrane helices in sarcoplasmic reticulum Ca^{2+}-ATPase: changes in cytoplasmic domain organization during isometric transition of phosphoenzyme intermediate and subsequent Ca^{2+} release. *J. Biol. Chem.* **279,** 2202–2210 (2004).
39. Møller, J. V. *et al.* Calcium transport by sarcoplasmic reticulum Ca^{2+}-ATPase. Role of the A domain and its C-terminal link with the transmembrane region. *J. Biol. Chem.* **277,** 38647–38659 (2002).
40. Orlowski, S. & Champeli, P. Kinetics of calcium dissociation from its high-affinity transport sites on sarcoplasmic reticulum ATPase. *Biochemistry* **30,** 352–361 (1991).
41. Inesi, G., Ma, H., Lewis, D. & Xu, C. Ca^{2+} occlusion and gating function of Glu 309 in the ADP-fluoroaluminate analog of the Ca^{2+}-ATPase phosphoenzyme intermediate. *J. Biol. Chem.* **279,** 31629–31637 (2004).
42. Otwinowski, Z. & Minor, W. Processing of X-ray diffraction data collected in oscillation mode. *Methods Enzymol.* **276,** 307–325 (1997).
43. Brünger, A. T. *et al.* Crystallography & NMR system: A new software suite for macromolecular structure determination. *Acta Crystallogr. D* **54,** 905–921 (1998).
44. Wang, W. *et al.* Structural characterization of the reaction pathway in phosphoserine phosphatase: crystallographic "snapshots" of intermediate states. *J. Mol. Biol.* **319,** 421–431 (2002).
45. Juul, B. *et al.* Do transmembrane segments in proteolysed sarcoplasmic reticulum Ca^{2+}-ATPase retain their functional Ca^{2+} binding properties after removal of cytoplasmic fragments by proteinase K? *J. Biol. Chem.* **270,** 20123–20134 (1995).
46. Kraulis, P. J. MOLSCRIPT: a program to produce both detailed and schematic plots of protein structures. *J. Appl. Crystallogr.* **24,** 946–950 (1991).
47. Kabsch, W. & Sander, C. Dictionary of protein secondary structure: pattern recognition of hydrogen-bonded and geometrical features. *Biopolymers* **22,** 2577–2637 (1983).

Supplementary Information accompanies the paper on **www.nature.com/nature**.

Acknowledgements We thank H. Suzuki for his contribution at the initial phase of this work. We acknowledge that the first crystals of $E2{\cdot}MgF_4^{2-}$ were made by Y. Tsubaki. Thanks are also due to M. Kawamoto, H. Sakai and E. Yamashita for data collection at SPring-8; N. Miyashita for making many movies; M. Takahashi and J. Tsueda for preparing figures; and Y. Ohuchi for computer programs. We are grateful to D. B. McIntosh for help in improving the manuscript and G. Inesi for communicating unpublished results to us. This work was supported in part by a Creative Science Project Grant from the Ministry of Education, Culture, Sports, Science and Technology, the Japan New Energy and Industry Technology Development Organization, and the Human Frontier Science Program.

Competing interests statement The authors declare that they have no competing financial interests.

Correspondence and requests for materials should be addressed to C.T. (ct@iam.u-tokyo.ac.jp). The atomic coordinates for $E1{\cdot}AlF_x{\cdot}ADP$ and $E2{\cdot}MgF_4^{2-}$ are deposited in the PDB under accession codes 1WPE and 1WPG, respectively.

©2004 Nature Publishing Group